Supplementary Information

Siberian vegetation growth intensifies monsoon precipitation in southern East Asia in late spring and early summer

Sang-Wook Yeh[1*], Byung-Ju Sohn[2*], Sae-Yoon Oh[1], Se-Yong Song[3], Jee-Hoon Jeong[4], Bin Wang[5,6], Renguang Wu[7] and Young-Min Yang[5]

[1]Department of Marine Science and Convergent Engineering, Hanyang University, Ansan, South Korea.

[2]School of Earth and Environmental Science, Seoul National University, Seoul, South Korea.

[3]Earth Research Institute, University of California, Santa Barbara, Santa Barbara, CA, USA

[4]Department of Oceanography, Chonnam National University, Gwangju, South Korea.

[5]Key Laboratory of Meteorological Disaster, Ministry of Education (KLME)/Joint International Research Laboratory of Climate and Environment Change (ILCEC)/Collaborative Innovation Center on Forecast and Evaluation of Meteorological Disasters (CIC-FEMD), Nanjing University of Information Science and Technology, Nanjing 210044, China.

[6]Department of Atmospheric Sciences and International Pacific Research Center, University of Hawaii, Honolulu, HI 96822, USA.

[7]School of Earth Sciences, Zhejiang University, Hangzhou, and Center for Monsoon System Research, and State Key Laboratory of Numerical Modeling for Atmospheric Sciences and Geophysical Fluid Dynamics, Institute of Atmospheric Physics, Chinese Academy of Sciences, Beijing, China.

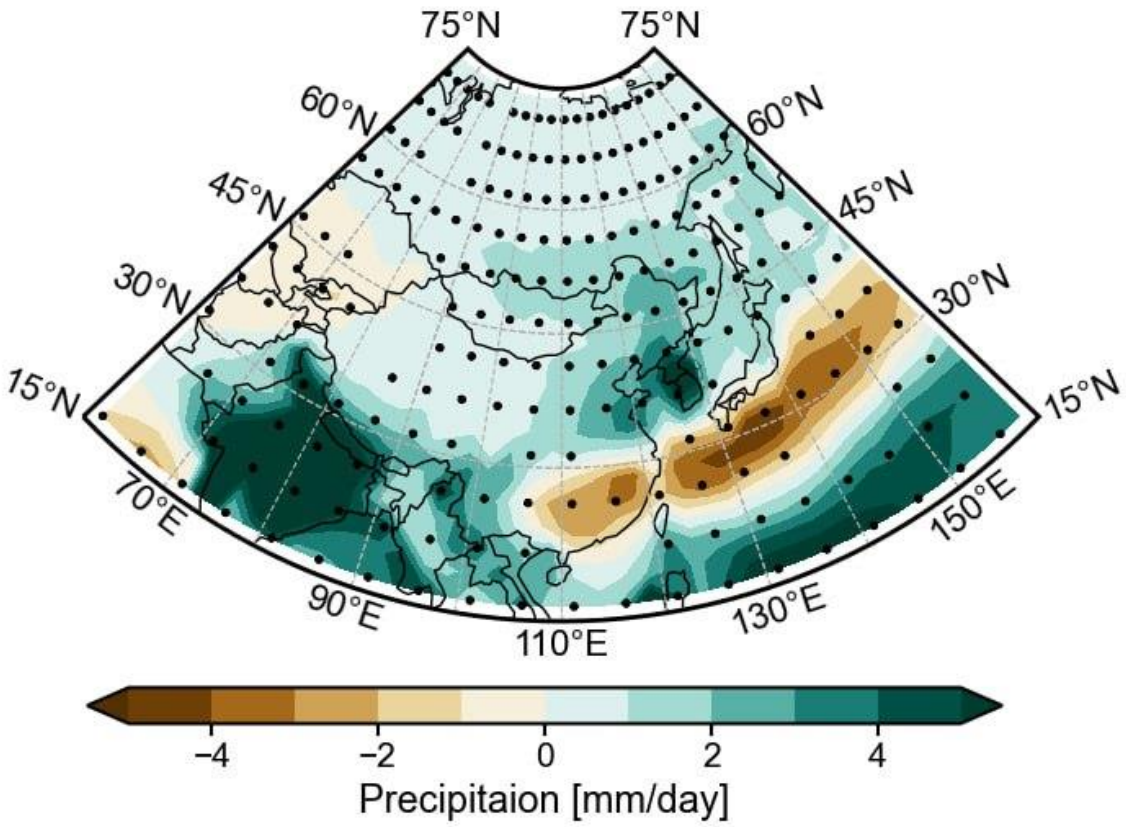

Supplementary Fig. 1 | The difference of climatological (1981-2010) mean precipitation between July-August and May-June (July-August minus May-June). Dot denotes the region where the difference is statistically significant at the 95% confidence level.

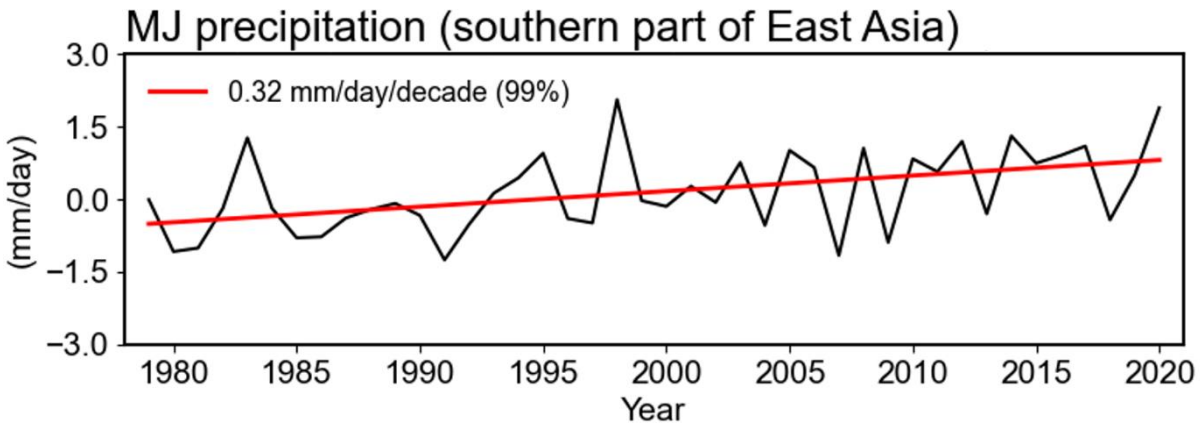

Supplementary Fig. 2 | Temporal evolution of precipitation in southern part of East Asia during May-June. Time-series of precipitation in the southern part of East Asia (105^{o}-140^{o}E, 22^{o}-36^{o}N) (black line) and its linear trend (red line) for 1979-2020 during MJ. Statistical significance is displayed in the left corner inside figure.

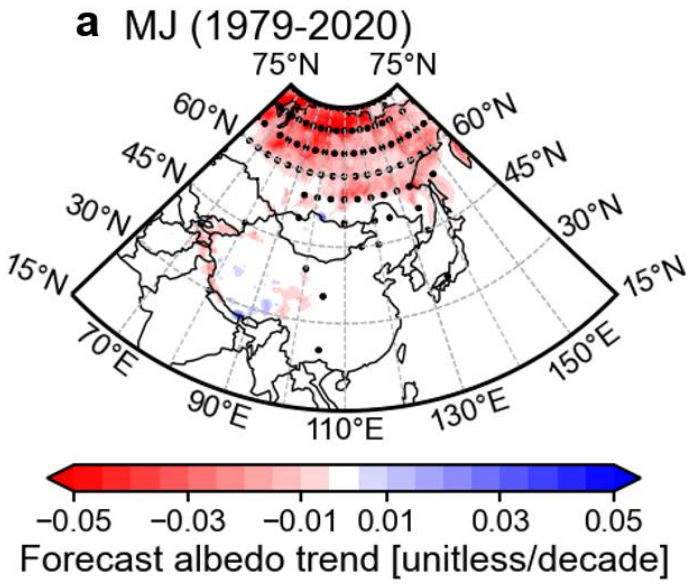

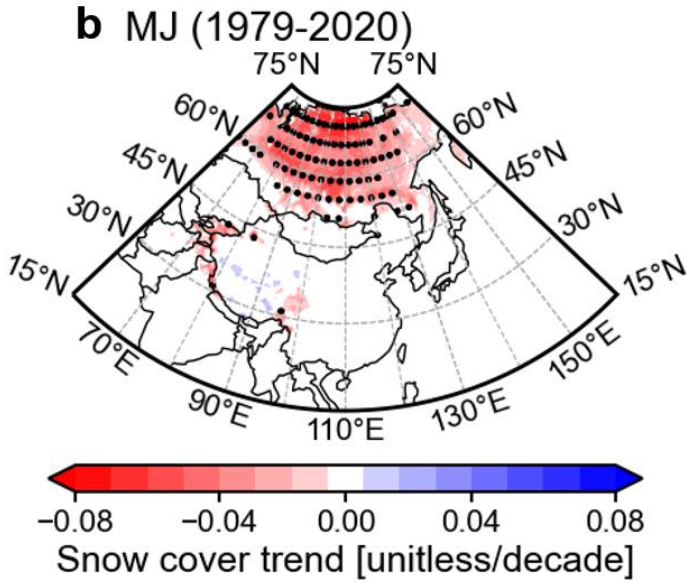

Supplementary Fig. 3 | Forecast albedo and snow cover linear trends during May-June. **a,** 1979-2020 forecast albedo linear trend during MJ. **b,** 1979-2020 snow cover linear trend during MJ. Stippling shows statistically significant areas at the 95% confidence level according to a Student's t-test.

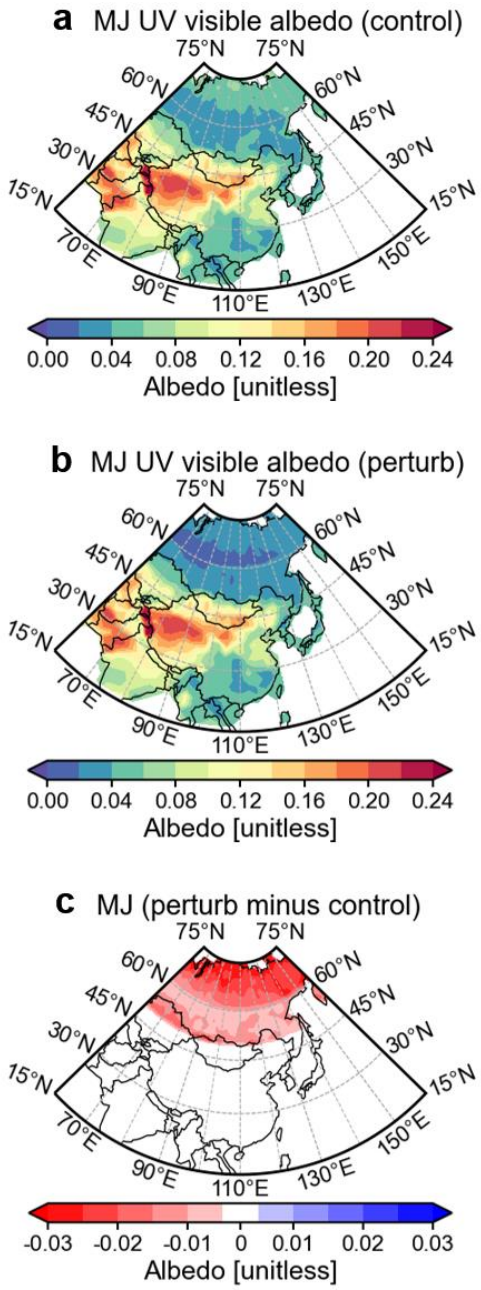

Supplementary Fig. 4 | Prescribed land surface albedo in the model experiment. a, Prescribed land surface snow-free albedo for visible direct shortwave radiation in the control experiment (shading, unitless) during MJ. **b,** Same as in **a** but for the albedo perturbation experiment. **c,** The difference in prescribed land surface snow-free albedo for visible direction shortwave radiation between the perturbation and control experiments during MJ.

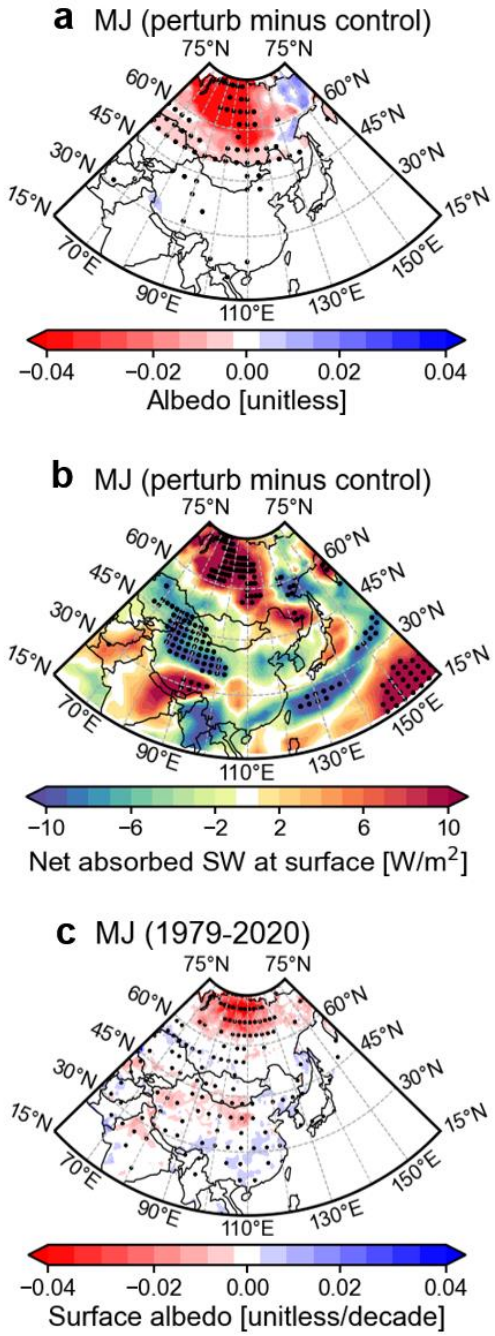

Supplementary Fig. 5 | Changes in the albedo and net absorbed shortwave radiation in the model experiment and the remote sensing. a, Changes in the albedo for the reduced land surface albedo in Siberia during MJ. **b,** Same as **a** but for the net absorbed shortwave radiation. **c,** 1982-2020 shortwave albedo linear trend during MJ in the remote sensing dataset obtained from CLARA-A3. Stippling shows statistically significant areas at the 95% confidence level according to a Student's *t*-test.

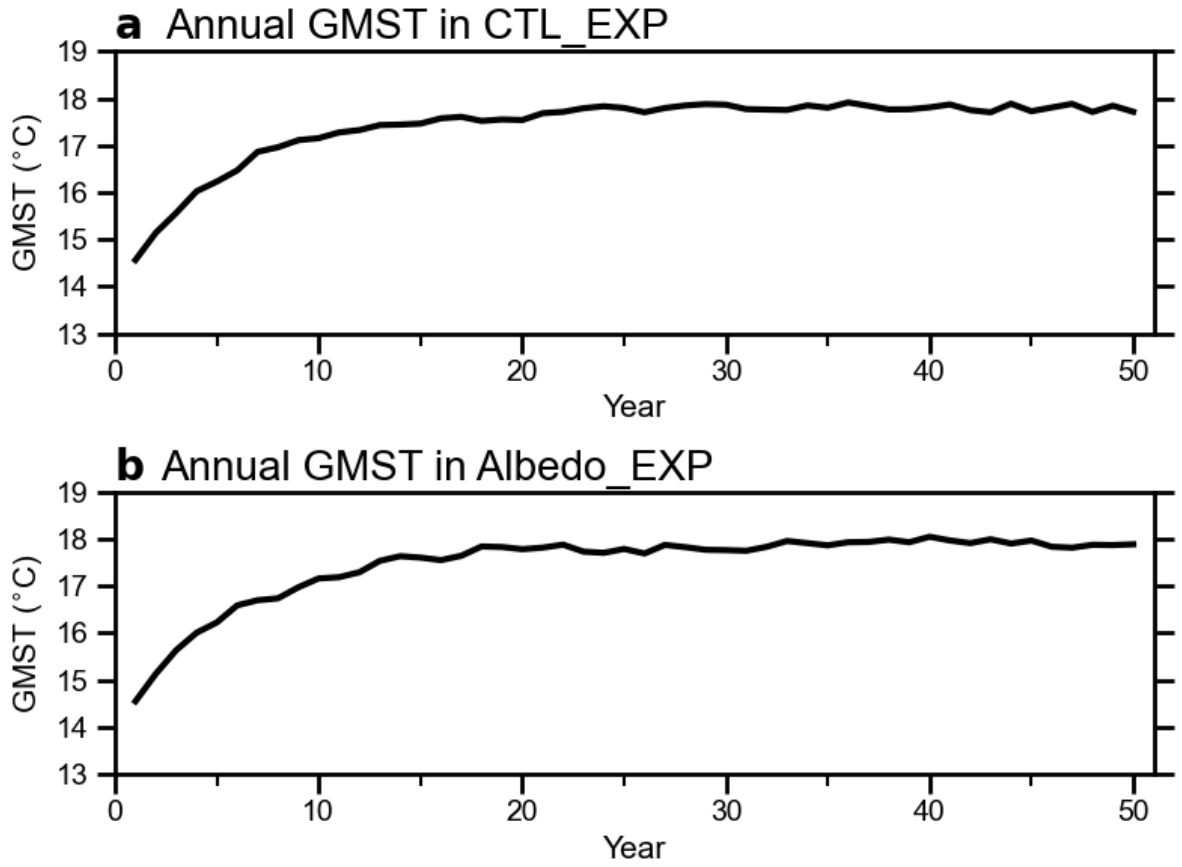

Supplementary Fig. 6 | Changes in the annual global mean surface temperature in the model experiment. Time-series of annual mean global mean surface temperature (GMST) in **a** CTL_Exp and **b** Albedo_Exp for the simulation period of 50 years.